Crystal Structures of Potent Thiol-Based Inhibitors Bound to Carboxypeptidase B[†,‡]

Marc Adler, Judi Bryant, Brad Buckman, Imadul Islam, Brent Larsen, Silke Finster, Lorraine Kent, Karen May, Raju Mohan, Shendong Yuan, and Marc Whitlow*

Berlex Biosciences, 2600 Hilltop Drive, P.O. Box 4099, Richmond, California 94804-0099

Received February 1, 2005; Revised Manuscript Received April 27, 2005

ABSTRACT: This paper presents the crystal structure of porcine pancreatic carboxypeptidase B (pp-CpB) in complex with a variety of thiol-based inhibitors that were developed as antagonists of activated thrombin-activatable fibrinolysis inhibitor (TAFIa). Recent studies have indicated that a selective inhibitor of TAFIa could enhance the efficacy of existing thrombolytic agents for the treatment of acute myocardial infarction, one of the most prevalent forms of heart attacks. Unfortunately, activated TAFIa rapidly degrades in solution and cannot be used for crystallographic studies. In contrast, porcine pancreatic CpB is stable at room temperature and is available from commercial sources. Both pancreatic CpB and TAFIa are zinc-based exopeptidases, and the proteins share a 47% sequence identity. The homology improves considerably in the active site where nearly all of the residues are conserved. The inhibitors used in this study were designed to mimic a C-terminal arginine residue, one of the natural substrates of TAFIa. The X-ray structures show that the thiol group chelates the active site zinc, the carboxylic acid forms a salt bridge to Arg145, and the guanidine group forms two hydrogen bonds to Asp255. A meta-substituted phenyl was introduced into our inhibitors to reduce conformational freedom. This modification vastly improved the selectivity of compounds against other exopeptidases that cleave basic residues. Comparisons between structures indicate that selectivity derives from the interaction between the guanidine group in the inhibitors and an acidic active site residue. The location of this acidic residue is not conserved in the various carboxypeptidases.

Acute myocardial infarction (AMI),[1] a type of heart attack, is one of the leading causes of death in the United States. Recombinant tissue-type plasminogen activator (t-PA) and other plasminogen activators have been widely used in thrombolytic therapy to treat patients suffering from AMI. Plasminogen activators work by converting plasminogen to plasmin, a serine protease that digests fibrin in blood clots. The critical factor that dictates efficacy of thrombolytic therapy for AMI patients is early, complete, and sustained blood flow through the previously clotted artery (*1*, *2*). During fibrinolysis, the exposure of C-terminal lysine and arginine residues on the Aα-chain of fibrin by plasmin accelerates the fibrinolysis by acting as binding sites for plasminogen and t-PA. This acceleration is offset by the presence of activated thrombin-activatable fibrinolysis inhibitor (TAFIa). TAFIa, which is also referred to as plasma carboxypeptidase B and carboxypeptidase U, removes the C-terminal lysine and arginine residues from fibrin. This cleavage depletes the available binding sites for plasminogen and tPA, thereby stabilizing the fibrin clot. An inhibitor of TAFIa should enhance the efficacy of existing thrombolytic agents for the treatment of AMI.

There are several published reports that support the utility of a TAFIa inhibitor. In a t-PA-induced whole blood clot lysis assay the addition of TAFIa significantly inhibited clot lysis. This effect can be overcome by the addition of a small protein carboxypeptidase inhibitor from potato (CPI). In addition, in the absence of exogenous TAFIa, CPI enhanced clot lysis in whole blood (*3*). The inhibitor CPI has been shown to decrease a fibrin clot size by 50% after 2 h in a rabbit jugular vein thrombosis model (*4*). In a second animal model, CPI was shown to reduce the time needed for t-PA to restore blood flow to an occluded aorta in a rabbit arterial thrombolysis model (*5*). The time to reperfusion was shortened from 23 min with t-PA alone to 7 min with the addition of CPI to the t-PA treatment (*5*). In the same study, t-PA alone resulted in 53% clot lysis in 60 min, while the combination of CPI and t-PA resulted in 89% clot lysis over the same time frame. Similar results were found in a rabbit arteriovenous shunt model in which the percent of clot lysis was measured at 90 min after the iv infusion of t-PA in the presence and absence of CPI (*6*). In the presence of CPI,

[1] Abbreviations: AMI, acute myocardial infarction; CpA, carboxypeptidase A; CpB, carboxypeptidase B; CpD, carboxypeptidase D (duck); CpN, carboxypeptidase N; CPI, carboxypeptidase inhibitor from potato; GEMSA, guanidinoethylmercaptosuccinic; HIC, hydrophobic interaction chromatography; MGTA, DL-2-mercaptomethyl-3-guanidinoethylthiopropanoic acid; pp-CpB, porcine pancreatic carboxypeptidase B; RMSD, root mean squared deviation; S1 pocket, the binding site for the residue preceding the proteolytic cleavage site; S1′ pocket, the binding site for the C-terminal Arg/Lys residue of the substrate; t-PA, tissue-type plasminogen activator; TAFIa, activated thrombin-activatable fibrinolysis inhibitor; Tris, tris(hydroxymethyl)aminomethane.

37% of the clot was lysed, whereas only 29% was lysed with t-PA alone. These studies support the hypothesis that an inhibitor of TAFIa could enhance the efficacy of existing thrombolytic agents for the treatment of AMI.

A detailed structure of human TAFIa would be an important aid for drug design. Unfortunately, activated human TAFI has a solution half-life of only 10 min at 37 °C (7), and it is not stable enough for crystallographic studies. Porcine pancreatic carboxypeptidase B (pp-CpB) becomes an attractive alternative protein for structural studies. Both pancreatic CpB and TAFIa are zinc-based exopeptidases, and pp-CpB shares a 47% sequence identity with human TAFIa. The homology improves considerably in the active site. There are only two conservative substitutions among the residues that line the presumptive binding site. Val203 and Leu247 in TAFIa are replaced by a Leu and Ile in pp-CpB. Furthermore, pp-CpB is stable at room temperature, and it is available from commercial sources.

The literature suggests two other homologues of TAFIa that may be suitable for structural studies, human pancreatic CpB (8) and a recently constructed chimera made from human TAFI and human pancreatic CpB (9). Unfortunately, the human pancreatic enzyme shows no better homology (47%) to TAFIa than the porcine pancreatic CpB (47%). Furthermore, both the chimeric enzyme and pure human pancreatic CpB share the same two amino acid substitutions in the active site (9; Val203 and Leu247). At the present time, porcine pancreatic CpB is the best alternative to TAFIa for our structural work.

There are two published reports of the structure of the inactive pro form of pancreatic CpB [1NSA (10); 1KWM (8)]. These structures include a 95-residue N-terminal activation segment. This N-terminal segment forms a compact globular domain that blocks access to the active site. It is not known if there are additional conformational rearrangements upon activation. There has been a recent report of the structure for the fully activated protein (11). However, the coordinates have not been released, and there is no direct comparison between the pro and activated forms.

This report presents the structure of an activated carboxypeptidase B structure and includes four structures from a series of enzyme/inhibitor complexes. The thiol-based inhibitors used in this study act as mimics for arginine. Most of these inhibitors are equipotent (3–10 nM) against human TAFIa, but they vary significantly in their selectivity against other homologous enzymes such as carboxypeptidase N (3–5000 nM). The structures provide valuable insight into the design of selective inhibitors for TAFIa.

EXPERIMENTAL PROCEDURES

What follows is the protocol for the crystallization of the porcine pancreatic carboxypeptidase B (pp-CpB)/MGTA complex. This procedure represents a refinement of earlier techniques in our laboratory, and it significantly improved the quality of the crystals. The reader is encouraged to contact the authors if they wish to know the details of the earlier crystallizations.

Compound Synthesis and Acquisition. DL-2-Mercaptoethyl-3-guanidinoethylthiopropanoic acid (MGTA) was purchased from Calbiochem (catalog no. 445825; San Diego, CA) and used without further purification. Compounds **1**,
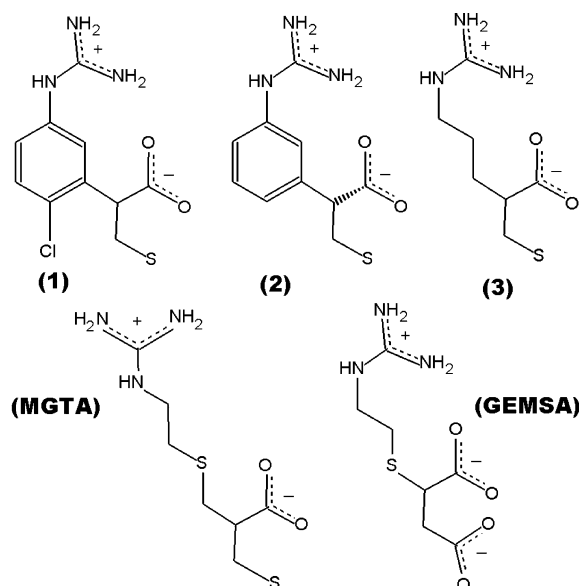

FIGURE 1: Covalent structures of the inhibitors discussed in this paper. All compounds were racemic mixtures except **2**, which purified as the *R* isomer.

2, and **3** (Figure 1) were synthesized as previously described [**1** and **2** (12); **3** (13)]. Compound **2** was prepared in chirally pure form. The X-ray crystallography confirmed the *R* conformation of the chiral center. Compounds **1** and **3** were prepared as racemates.

Enzyme Inhibition Assays. The assay for inhibition of porcine pancreatic CpB (Sigma, St. Louis, MO) was performed in a 96- or 384-well format adapted from published protocols (14, 15). Purified pp-CpB (2 nM) was incubated with test compounds in assay buffer (20 mM HEPES, pH 7.4, 150 mM NaCl, 5 mM CaCl$_2$) for 2 min prior to the addition of the 0.6 mM hippuryl-L-arginine substrate. After 30 min at room temperature, the amount of substrate hydrolyzed was determined by conversion of the product, hippuric acid, to a chromogen with sodium phosphate buffer, pH 8.3 (final concentration 0.8 mM), and cyanuric chloride/dioxane (final concentration 0.9% w/v) under a chemical fume hood. Following centrifugation of the microtiter plates and transfer of the supernatant to a clean plate, the absorbance of the supernatant is read at 382 nm. The IC$_{50}$ of the compound was determined using the four-parameter equation from an eight-point dose–response curve, each compound tested in duplicate.

The pp-CpB inhibition assay was modified for use with human plasma carboxypeptidase B (TAFI) and carboxypeptidase N (CpN). Purified TAFI (1.67 μM) must be activated immediately prior to use by a 15 min incubation in 20 mM HEPES, pH 7.4, 150 mM NaCl, 5 mM CaCl$_2$, and 0.1% BSA along with 10 nM thrombin and 50 nM thrombomodulin. Activation is then terminated with the addition of PPACK (1 μM). The final concentration of TAFIa was 9.2 nM. Human plasma CpN (3.16 μg/mL) (Enzyme Research Laboratories, South Bend, IN) was used without activation. The concentration of the substrate, hippuryl-L-arginine, was 1 mM for TAFI and 0.8 mM for CpN. The incubation time for TAFI was extended to 90 min. All other steps remain the same.

Protein Purification for Crystallization. Pp-CpB was obtained from Sigma (catalog no. C9584; St. Louis, MO)
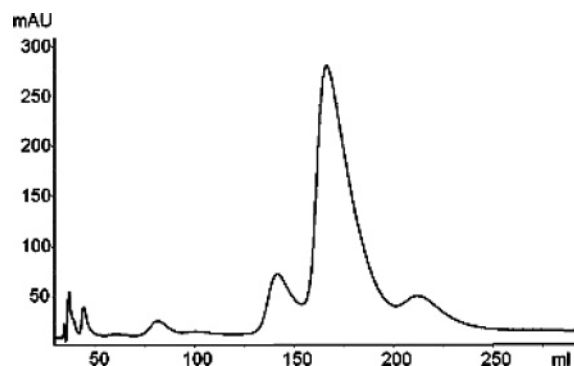
FIGURE 2: Chromatogram of porcine pancreatic carboxypeptidase B elution from the Toso-Haas phenyl-5PW column.

and purified by on a TSK-GEL phenyl 5PW column (catalog no. 14018; Tosohaas Biosciences, Montgomeryville, PA). pp-CpB (7.5 mg) was dissolved in 1.5 mL of 1.0 M ammonium sulfate, 10 mM tris(hydroxymethyl)aminomethane (Tris), and 50 mM NaCl, pH 7.6 (buffer A). A 2.1 cm × 25 cm TSK-GEL phenyl 5PW column (Phe-HIC) was equilibrated with 65% buffer A (1.0 M ammonium sulfate, 10 mM Tris, 50 mM NaCl, pH 7.0) and 35% buffer B (10 mM Tris, 50 mM NaCl, pH 7.0). The pp-CpB was loaded on the Phe-HIC column. The pp-CpB was eluted from the Phe-HIC column using a 60 min gradient from 65% buffer A:35% buffer B to 45% buffer A:55% buffer B at flow rates of 5.0 mL/min. All operations were done on an ÄKTA purifier system (Amersham Pharmacia Biotech, Buckinghamshire, U.K.). Three pp-CpB peaks eluted from the Phe-HIC column (Figure 2). The large central peak was collected, and MGTA was added to a final concentration of 1 mM.

Three Phe-HIC purification runs of pp-CpB were pooled and concentrated to 12.5 mL using a 10 mL stirred cell with a YM10 membrane (catalog no. 13622; Amicon/Millipore, Billerica, MA). The pp-CpB was then buffer-exchanged on a 2.1 cm × 20 cm Sepharose G-25 column into 10 mM Tris and 50 mM NaCl, pH 7.0, at flow rates of 5.0 mL/min. The concentration of the pp-CpB was estimated to 0.21 g/L from the UV spectra of the sample using a molar extinction coefficient of 75320 M^{-1} cm^{-1} [absence 0.1% = 2.179 calculated using Swiss-Prot ProtParam tool (*16*) and residues 96−401 in Swiss-Prot sequence entry P09955 (*17*)] at 280 nm.

Porcine Pancreatic Carboxypeptidase Complex Crystallization. A 10 mM solution of MGTA was dissolved in 10 mM Tris and 50 mM NaCl, pH 7.0, and the pH raised to around 7.0 with the addition of 1.5 equiv of sodium hydroxide. Twenty-two milliliters of 0.21 g/L pp-CpB was concentrated in a stirred cell concentrator with a YM-10 membrane (Amicon/Millipore, Billerica, MA). The volume was reduced to approximately 1.4 mL in the stirred cell, and 10 mM MGTA was added to a concentration of 1.0 mM. The concentration was continued in the Microcon YM-10, and the final volume was reduced to 140 μL. The concentration was estimated to be 28.6 g/L based on A_{280} of a 1:100 dilution in water.

The pp-CpB/MGTA complex crystallization was set up as hanging drops in Limbro 24-well plates. The reservoir contained from 0.15 to 0.30 M magnesium acetate, 0.1 M sodium cacodylate, pH 6.5, and 12−22% poly(ethylene glycol) 8000 (PEG 8000). Two microliters of pp-CpB/MGTA

was added to 2 μL of a reservoir solution and placed on a siliconized glass cover slip (Hampton Research, Aliso Viejo, CA) over that reservoir solution. The crystallization experiments were sealed with vacuum grease between the glass cover slip and the Limbro plate. Then pp-CpB seed crystals from an earlier preparation of pp-CpB with a proprietary inhibitor were placed in the wells. The best crystal grew in the reservoir that contained 0.30 M magnesium acetate, 0.1 M sodium cacodylate, pH 6.5, and 18.5% PEG 8000.

Porcine Pancreatic Carboxypeptidase B Data Collection. All defraction data were collected at the Stanford Synchrotron Radiation Laboratory, Palo Alto, CA, using beamline 7-1 for compounds **1**, **2**, and **3** and beamline 11-1 for MGTA. Beamline 7-1 was equipped with a Mar345 detector (marUSA Inc., Evanston, IL) and was set to a wavelength of 1.08 Å. Beamline 11-1 is equipped with a Quantum-315 (Area Detector System Corp., Poway, CA), and the wavelength was 1.009 Å. The crystal was transferred to a cryoprotection drop that contained 2 μL of its reservoir solution [20% poly-(ethylene glycol) 400, 18% PEG 8000, 0.25 M magnesium acetate, 0.1 M sodium cacodylate, pH 6.5] and 2 μL of pp-CpB/**1** (20.5 g/L) for 15 s. The crystal was then flash cryocooled in liquid nitrogen and transferred to an X-ray goniostat. During data collection, the crystal temperature was maintained at 100 K using an Oxford Cryostream (Oxford Cryosystems Ltd., Oxford, U.K.). Details of the data collection and unit cells appear in Table 1. The pp-CpB/**1**, pp-CpB/**2**, and pp-CpB/**3** data sets were processed with Mosflm (*18*) and Scala (*19*), and the pp-CpB/MGTA data set was processed with X-GEN (*20*, *21*).

Refinement of pp-CpB Structures. The first structure solved in this series was the pp-CpB/**2** complex. The initial coordinates were obtained by molecular replacement using MolRep (*22*) in the CCP4 program suite. The starting structure was derived from the catalytic domain of the procarboxypeptidase B [1NSA (*10*)]. All heteroatoms were stripped from the data set except the active site zinc. The MolRep solution indicated that there were three proteins in the asymmetric unit. The subunits are labeled with A-, B-, and C-chain letters based on the order the subunits came out in the MolRep solution. The starting model was then fit to the data using the rigid body refinement (*23*) with data that extended from 8.0 to 3.0 Å. Each subunit was allowed to move independently. Simulated annealing (*23*) was used to refine the structure as the higher resolution data was introduced in successive steps. The inhibitors were fit to the data once the resolution had been extended to 2.3 Å. Waters were added to the structure (*24*) in all subsequent steps. The programs X-PLOR 3.1 (*23*), O (*25*), and XtalView (*24*) were used in the refinement of the data. The residues are numbered using the system of Pereira et al. (*8*), which is based on the structural homology to carboxypeptidase A [3CPA (*26*)]. Subsequent structures were solved using direct replacement starting with the best available structure at the time. All other steps remained the same.

The final stages of refinement of data set **3** indicated that there were significant errors in the 2.33−2.20 Å resolution shell. Reexamination of the original images revealed two solvent rings centered at 3.59 and 2.23 Å. The low-resolution ice ring does not cause major problems, but the ring at 2.23 Å overwhelmed the nearby reflections. To correct this problem, the reflections between 2.29 and 2.20 Å were

Table 1: X-ray Diffraction Data and Refinement Statistics

data set	compound			
	1	**2**	**3**	MGTA
PDB entry code	1ZG7	1ZG8	1ZG9	1Z5R
measured inhibition constants (nM)				
TAFI	10	3	4	900
porcine pancreatic CpB	7	2	2	63
human CpN	4600	1700	3	63
diffraction data				
space group	$P2_12_12_1$	$P2_12_12_1$	$P2_12_12_1$	$P2_12_12_1$
beamline	SSRL 7-1	SSRL 7-1	SSRL 7-1	SSRL 11-1
wavelength (Å)	1.08	1.08	1.08	1.009
step size (deg)	0.35	1.0	1.0	0.25
exposure (s)	15	30	95	5
unit dimensions (Å)				
a	67.50	67.90	66.84	66.81
b	100.37	99.51	102.48	96.06
c	136.00	136.38	136.16	135.82
reflections	93605	61219	61762	161497
resolution range (Å)				
high	1.75 (1.75)[a]	2.00 (2.00)[a]	2.00 (2.00)[a]	1.40 (1.40)[a]
low	∼20 (1.83)	∼20 (2.09)	∼20 (2.09)	∼20 (1.46)
completeness (%)	99.9 (100)	96.6 (90.3)	91.3[b] (98.8)	93.9 (68.1)
redundancy	3.3 (3.3)	3.5 (3.4)	3.7 (3.6)	3.5 (3.2)
R_{sym}[c]	0.068 (0.36)	0.068 (0.35)	0.080 (0.25)	0.038 (0.28)
mean $I/\sigma(I)$	6.6 (1.7)	8 (2.0)	6.7 (3.0)	19 (2.0)
refinement				
resolution (Å)	8.0−1.75	8.0−2.00	8.0−2.00	8.0−1.40
no. of reflections				
input	92660	60238	57345[b]	160654
used ($F > 2\sigma$)	90906	59722	56660[b]	148794
R factor	0.208 (0.365)	0.214 (0.332)	0.203 (0.275)	0.175 (0.270)
R free	0.262 (0.338)	0.294 (0.324)	0.272 (0.315)	0.209 (0.263)
no. of non-hydrogen atoms	8019	7800	7830	8357
no. of residues	914	914	914	912
no. of solvent molecules	645	427	468	1046
no. of ligands + $3Zn^{2+}$	3	3	3	0
average B-factors	29.2	33.8	24.8	16.7
RMSD from ideal bond length (Å)	0.012	0.013	0.013	0.012
RMSD from ideal bond angles (deg)	1.81	1.87	1.82	1.86

[a] Statistics for the highest resolution shell of data are shown in parentheses. [b] A solvent ring prevented proper integration of peaks between 2.29 and 2.20 Å. The denoted statistics do not include peaks in this region. [c] $R_{sym} = \Sigma|I - \langle I \rangle|/\Sigma I$.

deleted. This reduced the completeness from 96.7% to 91.3% and removed 3330 reflections from the X-PLOR input. Further refinement of the structure produced a 2% decrease in *R* values. There was also significant improvement in the electron density for the bulk solvent. The structure deposited in the protein data bank, 1ZG9, is derived from this edited data set.

RESULTS

The initial crystallizations were performed with pp-CpB from a commercial source, and the protein was used without any further purification. This material was dissolved into a buffer of 10 mM Tris and 50 mM NaCl, pH 7.5, in the presence of 1 mM CpB inhibitor. The first set of crystals was obtained from 0.2 M magnesium acetate, 0.1 M sodium cacodylate, pH 6.5, and 20% PEG 8000 (Hampton Research Crystal Screen condition no. 18). These crystals were often twinned, and the diffraction data were difficult to analyze. Subsequent crystallizations were performed with pp-CpB that was purified by hydrophobic interaction chromatography (HIC). The protein separated into three peaks on a TSK-GEL phenyl 5PW column (Figure 2). The fractions from the large central peak were pooled and buffer exchanged into 10 mM Tris and 50 mM NaCl, pH 7.5. A CpB inhibitor,

such as MGTA, was added to prevent autolysis. The crystals grown from this preparation had fewer problems with twinning.

Considerable effort went into the development of a cryoprotectant for pp-CpB. Crystals frequently cracked when they were transferred to a cryodrop containing 20% ethylene glycol, 20% water, and 60% reservoir or a similar solution. Despite problems with twinning, the diffraction pattern from a single crystal could be indexed and reduced. The earlier data sets from complexes of pp-CpB/**1**, pp-CpB/**2**, and pp-CpB/**3** all exhibited some twinning, and occasionally the images were marred with ice rings. The problem was solved by preequilibrating the cryodrop against the reservoir solution in a hanging drop and reducing the time for soaking to 15−30 s. Noticeably, the *b* unit cell length was reduced from 100 to 96 Å in crystals prepared from this protocol (pp-CpB/MGTA and unpublished results). The quality of diffraction data also improved dramatically.

Table 1 lists the statistics for the four structures presented in this report. All four complexes crystallized in space group $P2_12_12_1$ with approximate unit cells of $a = 67$ Å, $b = 100$ Å, and $c = 136$ Å. There were three protein molecules in the asymmetric unit. The resolutions of the data sets were 1.75 Å for compound **1**, 2.0 Å for **2** and **3**, and 1.4 Å for

MGTA. The values of R and R free from the refinements were 0.21 and 0.26 (**1**), 0.21 and 0.29 (**2**), 0.20 and 0.27 (**3**), and 0.17 and 0.21 (MGTA). Table 1 also lists the measured inhibition constants for these inhibitors against several carboxypeptidases. Figure 3 provides a stereoview of the active site of enzyme/inhibitor complex along with the electron density for three of the inhibitors: **1**, **2**, and **3**. The electron density for the fourth inhibitor, MGTA, was weak and inconsistent with the geometry of the compound near the zinc. Therefore, the structure is reported without the inhibitor in the active site.

The overall fold of activated pp-CpB is identical to other carboxypeptidases in this family [1NSA (*10*); 1KWM (*8*); 3CPA (*26*)]. In the highest resolution structure, pp-CpB/MGTA, only three residues lie outside the low energy region of the Ramachandran plot, Ser199, Ile247, and Asp273. All three residues line the arginine binding site (S1′), and two residues are in close proximity to the cis peptide bonds (Tyr198, Tyr206, and Asp273). The side chains in the highest resolution structure appear to have a single stable conformation. The average B-factors of the main chain atoms of the protein are consistently low (13.6 Å^2). There were several patches of elevated B-factors (>20 Å^2) near the crystal contact surfaces: A207−A242, B54−B60, C85−C104, etc. These perturbations varied from subunit to subunit.

The surface loop that covers the S1′ binding site, residues 245−249, consistently showed elevated B-factors in all of the structures. The B-factors for this loop are nearly twice as high as the rest of the protein, and there was poor electron density for Tyr248 in all the structures. It is interesting to compare these results to structures of the homologous protein, carboxypeptidase A (CpA). There are two published structures of CpA complexed to peptide-based inhibitors [4CPA (*27*); 1DTD (*28*)]. The loop from 245 to 249 forms several contacts with both the S1′ and S1 residues of the inhibitor. Notably, the B-factors for this loop are comparable to the rest of the protein. These results indicate that the loop from 245 to 249 may act as a flap that opens and releases the cleaved residue from the S1′ site.

Comparisons of Activated and Pro Forms of pp-CpB. The structure of activated pp-CpB closely aligns with published structure of the proenzyme [1NSA (*10*)]. The root mean squared deviation (RMSD) of the C$^\alpha$ atoms is 0.45 Å. This compares favorably with the 0.35 Å RMSD between the three different subunits of activated pp-CpB within the asymmetric unit.

There are some noticeable differences in the packing of the side chains within the active site. In the proenzyme, Tyr248 points away from the active site. In our structures, the corresponding phenol ring points inward toward the zinc ion (Figure 3A). Similar displacements of this phenol ring have been observed in CpA (*29−31*). However, the electron density for this side chain is always weak, and the B-factors are high. Other conformational changes involve the side chains of residues Arg145, Arg127, and Glu270. The perturbations are comparable to shifts seen in our structures with different inhibitors. The results imply that these changes are induced by ligand binding and not by activation.

The Swiss-Prot data bank lists two sequences for porcine pancreatic CpB. The more recent entry (*32*) was obtained from gene sequencing. The older entry (*17*) is based on the X-ray structure of Coll et al. [1NSA (*10*)]. Coll et al. derived

the sequence of the catalytic domain directly from the X-ray data that extended out to 2.3 Å. At this resolution, the electron density is often blurry for the surface side chains. When the project was initiated in our laboratory, there was still no gene sequence available. The subsequent report of a gene sequence (*33*) showed a discrepancy in 34 of the 306 residues.

To resolve this issue, we solved our highest resolution structure (1.4 Å, pp-CpB/MGTA) using the sequence of 1NSA. For 19 residues, there is a difference in shape for the residues reported in the X-ray and gene sequences. In 17 positions, the electron density clearly indicated that the gene sequence was correct (Figure 3D,E). The two remaining positions were Ser57 → Pro and a Ser237 → Lys. There was not enough electron density to confirm the larger side chain. For the remaining 15 sites, it was not possible to distinguish between residues that had the same shape, such as Asp45 → Asn and Thr301 → Val. However, the gene sequence was adopted for the entire protein and is used in the deposited coordinates.

*Binding Interactions of Compound **1** with Porcine Pancreatic CpB.* Figure 4A shows the active site of pp-CpB in complex with inhibitor **1**. The thiol group chelates the zinc (2.2 Å) and becomes part of tetrahedral coordination sphere that includes residues His69, Glu72, and His196. The free carboxylic acid forms a tight salt bridge with the N$^\eta$'s of Arg145 (2.8 Å). The inhibitor forms a second salt bridge through N$^\epsilon$ (3.0 Å) and N$^\eta$ (2.7 Å) atoms to Asp256 at the base of the S1′ pocket. The phenyl ring points toward Leu203 (3.6 Å), and the chlorine is in close contact with C$^\beta$ and C$^\gamma$ of Glu120 (3.4 Å). The chiral carbon in **1** has R stereochemistry. This chiral center is inverted when compared to the naturally occurring L-Arg.

Although pp-CpB and TAFIa have limited sequence homology (47%), the residues in the active site are well conserved. The crystal structure provides insights into how the sequence differences might affect binding. There are two conservative substitutions in the residues that line the S1′ pocket (Figures 3 and 4): Leu203 and Ile247 in pp-CpB are replaced by Val and Leu. Further away from the active site, His201 in TAFIa replaces Met201. Our inhibitors have no direct contact with Met201 (5.7 Å), and there are only weak interactions with Ile247 (4.6 Å). There is one close contact (3.6 Å) between the phenyl ring of the inhibitor and the end of the Leu203 side chain (Figure 4A). In theory, the addition of a methyl group adjacent to the chlorine in **1** should create a compound that is selective for Val203 in TAFIa versus the larger Leu in pp-CpB, but no experiments have been performed. In general, our compounds show similar inhibition constants for these homologous proteins (Table 1), and presumably, the inhibitors adopt the same conformation in both enzymes.

Comparisons between Different Ligands. Figure 1 shows the covalent structure of the inhibitors used in this study. The measured inhibition constants are included in Table 1 along with a summary of the X-ray refinement statistics. The bound conformation of three of the inhibitors appears in Figure 3. The electron density indicated that the enzyme selectively binds the R conformation of all three compounds. Compound **3** is essentially an arginine residue with a mercaptomethyl group replacing the free amine. Two other inhibitors, **1** and **2**, share the same functional groups and
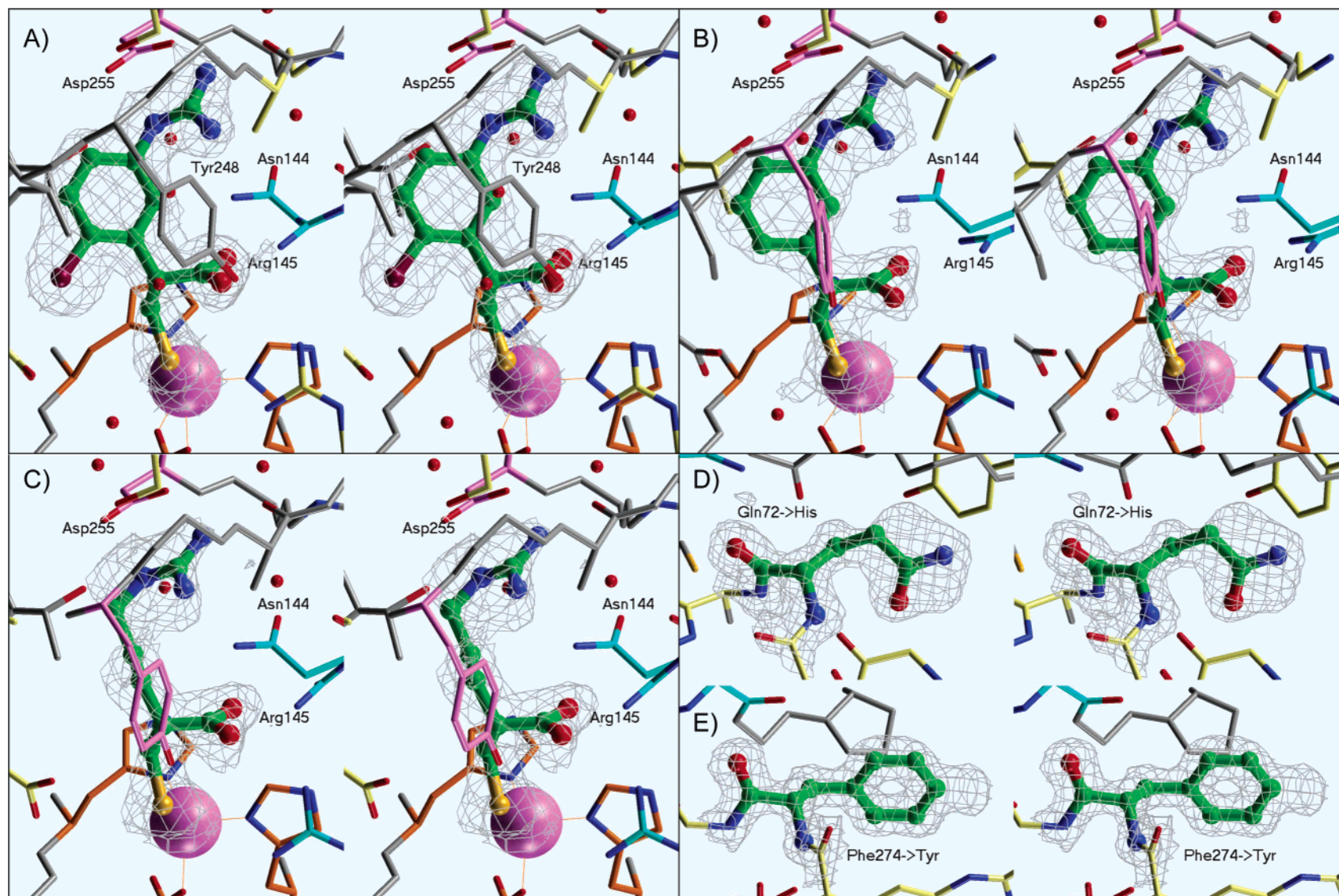
FIGURE 3: Divergent stereoview of the active site pp-CpB in complex with three different inhibitors: (A) **1**, (B) **2**, and (C) **3**. Panel D shows residue 72 from the pp-CpB/MGTA structure. The X-ray sequence lists a glutamine at this position (*17*), whereas the gene sequence lists a histidine (*32*). Panel E displays position 274 (X-ray, Phe; gene, Tyr). The density and coordinates in panels D and E were refined using the X-ray sequence. The electron density is contoured at 1σ using the blob option in XtalView with a 2 Å radius. The inhibitors or highlighted residues are displayed with green carbon atoms. The three residues that chelate the zinc are shown in orange: His69, Glu72, and His196. Other residues are colored by their contact with the inhibitor: yellow for any contact under 3.5 Å, pink or cyan depending on if an oxygen or a nitrogen forms a hydrogen bond with the inhibitor (<3.2 Å). Backbone carbonyls and nitrogens were not properly displayed unless the atoms were in close proximity to the inhibitor (<4.0 Å). Similarly, side chains were not displayed unless at least one atom was within 5.5 Å for panel A or 4 Å for the other panels.
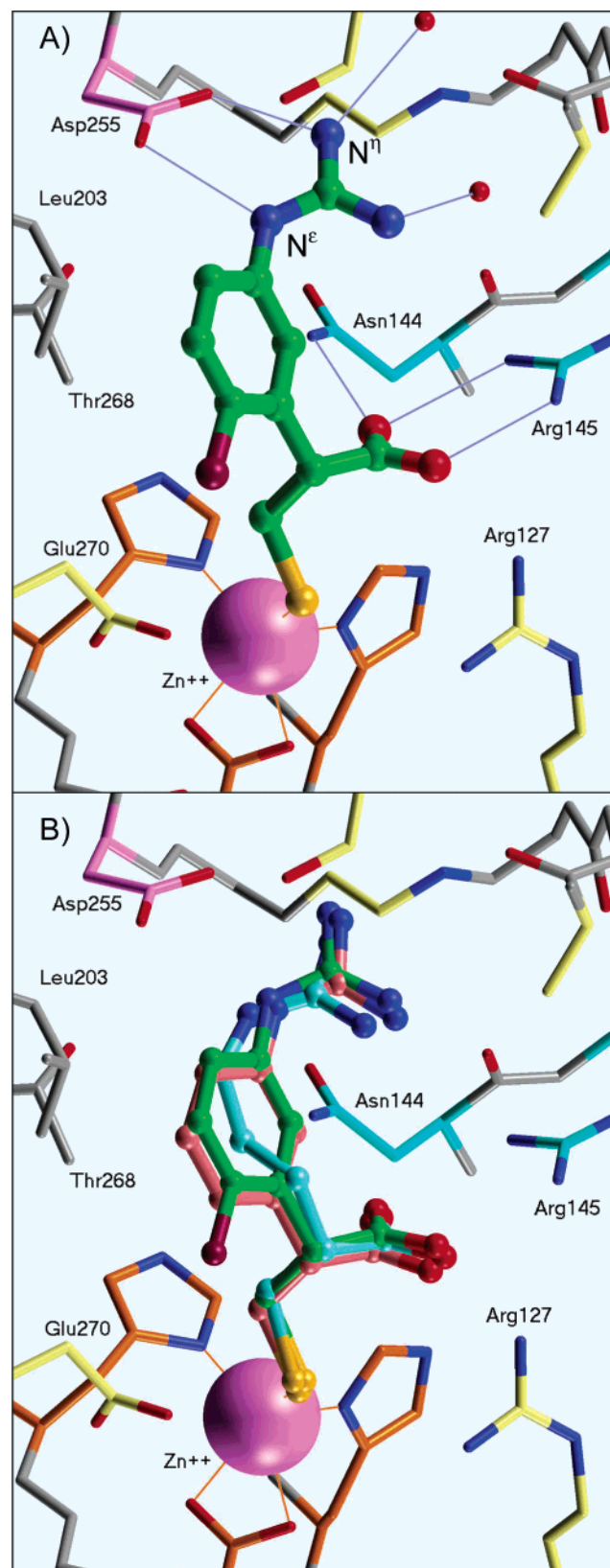
FIGURE 4: (A) Active site of the pp-CpB/**1** complex showing the hydrogen bonds to the inhibitor. Compound **1** is colored in green and its chlorine atom is shown in purple. (B) Superimposed structures of compounds **1**, **2**, and **3**. The carbon atoms of the inhibitors are colored green, peach, and cyan, respectively. Coloring and display of the residues are the same as in Figure 3.

have similar potency against TAFIa (3−10 nM). Compounds **1**, **2**, and **3** all have the same number of carbons between

the thiol and the guanidinium group. The compound MGTA differs from **3** by the insertion of sulfur into the methylene side chain (Figure 1). The insertion results in more than a 100-fold loss of affinity for TAFIa (900 nM) and a 30-fold drop against pp-CpB (63 nM). This indicates that the enzyme is sensitive to distance between the guanidine and the zinc binding moiety.

Unfortunately, the low potency of MGTA made it difficult to determine the structure for the inhibitor even though the data extended out to 1.4 Å. The A- and C-subunits had clear density for the guanidinium group, but the density became discontinuous toward the zinc ion, and there was almost no electron density in the acid binding site (data not shown). The electron density in the active site of the B-subunit was not interpretable. Several attempts were made to fit either the *R* or *S* forms of MGTA using the thiol or carboxylic acid chelated to the zinc, and L-arginine was also tried, but nothing gave an acceptable fit. The results imply that there are multiple binding modes. The deposited coordinates do not include an inhibitor.

Figure 4B shows the superimposed structures of compounds **1**, **2**, and **3** bound to pp-CpB. There is a close alignment in the key functional groups. The RMSD for the thiol group is 0.25 Å and 0.34 Å for the carboxylic acid. There is slightly more variation in the position of the N^η atoms (0.48 Å). Comparisons between all of the structures indicate that the guanidinium is displaced by about 0.5 Å when comparing the phenyl-based compounds, **1** and **2**, with the two saturated ones, **3** and MGTA. There is a corresponding 0.25 Å shift in the side chain of Asp255. This shift preserves the hydrogen bonds.

There were often minor variations in conformation of the active sites of the three proteins within the same crystal. These differences frequently stemmed from ambiguities in the electron density, and the problems became more pronounced in the lower resolution data (**2** and **3**). Furthermore, the electron density in **3** indicated that the inhibitor had multiple conformations. In particular, the inhibitor in the A-subunit appeared to have a second conformation with both N^η atoms interacting with Asp255. However, no single conformation provides a satisfactory fit to the $2F_o - F_c$ map (data not shown).

In general, crystal packing forces do not perturb the conformation of the active site cleft. There is, however, some contact between C^α of Tyr248 in the B-subunit and the Asn101 side chain in subunit C (5 Å). This crystal contact did not measurably perturb the inhibitor.

DISCUSSION

Potent Inhibitors of Carboxypeptidase B. Three of the inhibitors used in this study exhibit nanomolar potency to CpB: **1**, **2**, and **3**. The X-ray structures reveal a common binding mode (Figure 4B). The thiol chelates the zinc; the carboxylic acid and guanidinium groups form salt bridges to Arg145 and Asp255, respectively. Each inhibitor has five carbon atoms between the sulfur and guanidine groups. With the exception of the mercapto substituent, these inhibitors are close mimics of arginine and probably bind in similar fashion as the natural substrate. None of the inhibitors had hydrophilic interactions with Glu270, a catalytically important residue (*34*). Presumably, favorable interactions with this residue would increase the potency of the compounds.
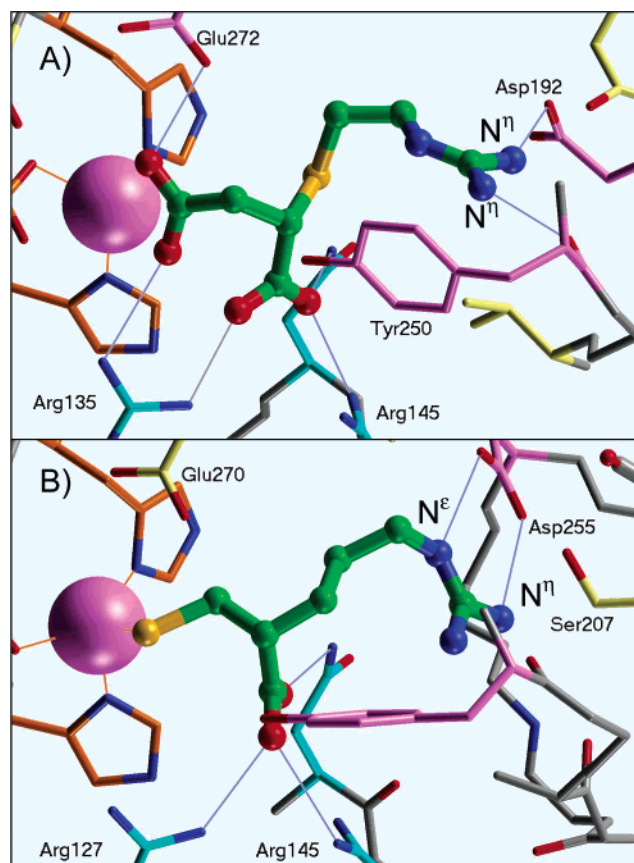
FIGURE 5: (A) Bound conformation of GEMSA in CpD [1H8L (*35*)] with the hydrogen bonds drawn as lines. (B) Compound **3** in pp-CpB using the same orientation as in panel A. Coloring and display of the residues are the same as in Figure 3.

Design-Selective Inhibitors for TAFIa verses Carboxypeptidase N. Carboxypeptidase N (CpN) is a critical enzyme in the complement system, and inhibition of this enzyme will presumably result in undesirable side effects. CpN is another zinc exopeptidase that has a specificity for C-terminal arginines and lysines. Therefore, it is important to design inhibitors that are selective for TAFIa over CpN. The initial lead compound in the series, **3**, is equipotent against CpN, TAFIa, and CpB (Table 1).

Valuable information can be gained from the published structure of carboxypeptidase D (CpD) with the compound guanidinoethylmercaptosuccinic (GEMSA, Figure 1), bound in the active site [1H8L (*35*)]. CpD shares 50% sequence identity with human CpN, and the homology improves considerably in the active site. The inhibitor GEMSA is similar to compound **3** except the thiol group has been replaced by a carboxylic acid. The bound conformation of the inhibitor is shown in Figure 5A. The guanidine in GEMSA binds the protein by forming hydrogen bonds through the two N^η atoms with an O^ϵ of Asp192 and the backbone carbonyl of Tyr250. (The homologous residues in CpB are Ser207 and Tyr248.) In our structure the guanidine moiety forms H-bonds through the N^ϵ and N^η atoms (Figure 5A). The two different binding modes in CpB and CpD force a change in the methylene side chain of the inhibitor. GEMSA has a gauche bond between C^γ and C^δ. Compound **3** is all-trans through the C^δ, and the $C^\delta-N^\epsilon$ bond is bent.

The introduction of an aromatic ring into the side chain for compound **2** forces the chain to adopt an extended

conformation (Figure 4). The results indicate that the *R* diastereomer of **2** has a 600-fold selectivity of TAFIa over CpN. The compound would have to fully extend in order to bind CpD through N^η atoms, and this would increase the distance between the thiol and the guanidinium group by about 1.5 Å. Our modeling techniques have failed to find a conformation that maintains the interactions at the three key sites. The selectivity of our inhibitors may stem from the hydrogen bonds formed by the guanidine headgroup.

Our crystal structures provide important information on the active site cleft of pp-CpB. The bound conformations of **1**, **2**, and **3**, delineate the distances between the conserved residues in the zinc, anion, and cation binding sites. These structures also indicate that there is ample room for cyclic structures in the S1′ pocket. It is our plan to use pp-CpB as a model protein for human TAFIa. This approach mirrors the work of Stubbs et al. (*36*), who examined selective Xa inhibitors using bovine trypsin. The ideas garnered from our pp-CpB structures should translate into the design of selective inhibitors for human TAFIa.

ACKNOWLEDGMENT

REFERENCES

1. Anderson, H. V., and Willerson, J. T. (1993) Thrombolysis in acute myocardial infarction, *N. Engl. J. Med. 329*, 703–709.
2. Lenderink, T., Simoons, M. L., Van Es, G.-A., Van de Werf, F., Verstraete, M., and Arnold, A. E. R. (1995) Benefit of thrombolytic therapy is sustained throughout 5 years and is related to TIMI perfusion grade 3 but not grade 2 flow at discharge, *Circulation 92*, 1110–1116.
3. Redlitz, A., Tan, A. K., Eaton, D. L., and Plow, E. F. (1995) Plasma carboxypeptidases as regulators of the plasminogen system, *J. Clin. Invest. 96*, 2534–2538.
4. Minnema, M. C., Friederich, P. W., Levi, M., von dem Borne, P. A., Mosnier, L. O., Meijers, J. C., Biemond, B. J., Hack, C. E., Bouma, B. N., and ten Cate, H. (1998) Enhancement of rabbit jugular vein thrombolysis by neutralization of factor XI as an anti-fibrinolytic factor. In vivo evidence for a role of factor XI as an anti-fibrinolytic factor, *J. Clin. Invest. 101*, 10–14.
5. Klement, P., Liao, P., and Bajzar, L. (1999) A novel approach to arterial thrombolysis, *Blood 94*, 2735–2743.
6. Refino, C. J., DeGuzman, L., Schmitt, D., Smyth, R., Jeet, S., Lipari, M. T., Eaton, D., and Bunting, S. (2000) Consequences of inhibition of plasma carboxypeptidase B on in vivo thrombolysis, thrombosis and hemostasis, *Fibrinolysis Proteolysis 14*, 305–314.
7. Boffa, M. B., Wang, W., Bajzar, L., and Nesheim, M. E. (1998) Plasma and recombinant thrombin-activatable fibrinolysis inhibitor (TAFI) and activated TAFI compared with respect to glycosylation, thrombin/thrombomodulin-dependent activation, thermal stability and enzymatic properties, *J. Biol. Chem. 273*, 2127–2135.
8. Barbosa Pereira, P. J., Segura-Martin, S., Oliva, B., Ferrer-Orta, C., Avilés, F.-X., Coll, M., Gomis-Rueth, F.-X., and Vendrell, J. (2002) Human procarboxypeptidase B: Three-dimensional structure and implications for thrombin-activatable fibrinolysis inhibitor (Tafi), *J. Mol. Biol. 321*, 537.
9. Marx, P. F., Havik, S. R., Marquart, J. A., Bouma, B. N., and Meijers, J. C. (2004) Generation and characterization of highly stable form of activated thrombin-activable fibrinolysis inhibitor, *J. Biol. Chem. 279*, 6620–6628.
10. Coll, M., Guasch, A., Avilés, F.-X., and Huber, R. (1991) Three-dimensional structure of porcine procarboxypeptidase B: A structural basis of its inactivity, *EMBO J. 10*, 1–9.
11. Polla, M. O., Tottie, L., Norden, C., Linschoten, M., Musil, D., Trumpp-Kallmeyer, S., Aukrust, I. R., Ringom, R., Holm, K. H., Neset, S. M., Sandberg, M., Thurmond, J., Yu, P., Hategan, G., and Anderson, H. (2004) Design and synthesis of potent, orally

active, inhibitors of carboxypeptidase U (TAFIa), *Bioorg. Med.* 12, 1151−1175.

12. Schering PCT published patent application WO/03/080631.

13. Ondetti, M. A., Condon, M. E., Reis, J., Sabo, E. F., Cheung, H. S., and Cushman, D. W. (1979) Design of potent inhibitors of carboxypeptidase A and B, *Biochemistry 18*, 1427−1430.

14. Suzuki, S., Hachimori, Y., and Yaoeda, U. (1970) Spectrophotometric determination of glycine with 2,4,6-trichloro-*s*-triazine, *Anal. Chem. 42*, 101−103.

15. Hendricks, D., van Sande, M., and Scharpe, S. (1986) Colorimetric assay for carboxypeptidase N in serum, *Clin. Chim. Acta 157*, 103−108.

16. http://www.expasy.ch/tools/protparam.html.

17. http://us.expasy.org/cgi-bin/niceprot.pl?P09955.

18. Leslie, A. G. W. (1990) *Crystallographic Computing*, Oxford University Press, Oxford.

19. Collaborative Computational Project 4 (1994) *Acta Crystallogr. D50*, 760−763.

20. Howard, A. J., Gilliland, G. L., Finzel, B. C., Poulos, T. L., Ohlendorf, D. H., and Salemme, F. R. (1987) Use of an imaging proportional counter in macromolecular crystallography, *J. Appl. Crystallogr. 20*, 383−387.

21. Accelrys Inc. X-GEN product information (July 1, 2002) http://www.accelrys.com/cerius2/c2xgen.html.

22. Navaza, J. (1994) *Acta Crystallogr. A50*, 157−163.

23. Brünger, A. (1993) X-PLOR: A System for X-ray Crystallography and NMR, Version 3.1, Yale University Press, New Haven, CT.

24. McGee, D. E. (1992) *J. Mol. Graphics 10*, 44−46.

25. Jones, T. A., Zou, J. Y., Cowan, S. W., and Kjeldgaard, M. (1991) Improved methods for binding protein models in electron density maps and the location of errors in these models, *Acta Crystallogr. A47*, 110−119.

26. Christianson, D. W., and Lipscomb, W. N. (1986) X-ray crystallographic investigation of substrate binding to carboxypeptidase A at subzero temperature, *Proc. Natl. Acad. Sci. U.S.A. 83*, 7568−7572.

27. Rees, D. C., and Lipscomb, W. N. (1982) Refined crystal structure of the potato inhibitor complex of carboxypeptidase A at 2.5 Å resolution, *J. Mol. Biol. 160*, 475−498.

28. Reverter, D., Fernandez-Catalan, C., Baumgartner, R., Pfander, R., Huber, R., Bode, W., Vendrell, J., Holak, T. A., and Avilés, F.-X. (2000) Structure of a novel leech carboxypeptidase inhibitor determined free in solution and in complex with human carboxypeptidase A2, *Nat. Struct. Biol. 7*, 322−328.

29. Guasch, A., Coll, M., Avilés, F. X., and Huber, R. (1992) Three-dimensional structure of porcine pancreatic procarboxypeptidase A. A comparison of the A and B zymogens and their determinants for inhibition and activation, *J. Mol. Biol. 224*, 141−157.

30. García-Sáez, I., Reverter, D., Vendrell, J., Avilés, F. X., and Coll, M. (1997) The three-dimensional structure of human procarboxypeptidase A2. Deciphering the basis of the inhibition, activation and intrinsic activity of the zymogen, *EMBO J. 16*, 6906−6913.

31. Van Aalten, D. M., Chong, C. R., and Joshua-Tor, L. (2000) Crystal structure of carboxypeptidase a complexed with D-cysteine at 1.75 Å−Inhibitor-induced conformational changes, *Biochemistry 39*, 10082−10089.

32. http://us.expasy.org/cgi-bin/niceprot.pl?Q9XSP3.

33. Ventura, S., Villegas, V., Sterner, J., Larson, J., Vendrell, J., Hershberger, C. L., and Avilés, F.-X. (1999) Mapping the pro-region of carboxypeptidase B by protein engineering. Cloning, overexpression, and mutagenesis of the porcine proenzyme, *J. Biol. Chem. 274*, 19925−19933.

34. Nau, H., and Riordan, J. F. (1975) Gas chromatography−mass spectrometry for probing the structure and mechanism of action of enzyme active sites. The role of Glu-270 in carboxypeptidase A, *Biochemistry 14*, 5285−5294.

35. Aloy, P., Companys, V., Vendrell, J., Avilés, F.-X., Fricker, L. D., Coll, M., and Gomis-Ruth, F. X. (2001) The crystal structure of the inhibitor-complexed carboxypeptidase D domain II and the modeling of regulatory carboxypeptidases, *J. Biol. Chem. 276*, 16177−16184.

36. Stubbs, M. T., Huber, R., and Bode, W. (1995) Crystal structures of factor Xa specific inhibitors in complex with trypsin: structural grounds for inhibition of factor Xa and selectivity against thrombin, *FEBS Lett. 375*, 103−107.